Award Number: 01HQGR0048

MAGNITUDE SCALING OF THE FORWARD RUPTURE DIRECTIVITY PULSE IN NEAR-FAULT GROUND MOTIONS

FINAL REPORT, MARCH 28, 2003

Paul Somerville

URS Group, Inc.

566 El Dorado Street
Pasadena, CA 91101

Tel: (626) 449-7650
Fax: (626) 449-3536

Email: paul_somerville@urscorp.com

Research supported by the U.S. Geological Survey (USGS), Department of the Interior, under award number 01HQGR0048. The views and conclusions contained in this document are those of the authors and should not be interpreted as necessarily representing the official policies, either expressed or implied, of the U.S. Government.

MAGNITUDE SCALING OF THE FORWARD RUPTURE DIRECTIVITY PULSE IN NEAR-FAULT GROUND MOTIONS

Award Number: 01HQGR0048

Principal Investigator: Paul Somerville

URS Group, Inc.
566 El Dorado Street
Pasadena, CA 91101
Tel: (626) 449-7650, Fax: (626) 449-3536
Email: paul_somerville@urscorp.com

ABSTRACT

Current ground motion models all assume monotonically increasing spectral amplitude at all periods with increasing magnitude. However, near fault recordings from recent earthquakes confirm that the near-fault fault-normal forward rupture directivity velocity pulse is a narrow band pulse whose period increases with magnitude. This magnitude dependence of the period of the near fault pulse is expected from theory, because the period of the pulse is related to source parameters such as the rise time (duration of slip at a point on the fault) and the dimensions of asperities, which generally increase with magnitude. This magnitude dependence of the pulse period causes the response spectrum to have a peak whose period increases with magnitude, such that the near-fault ground motions from smaller earthquakes may exceed those of larger earthquakes at intermediate periods (around 1 second).

The report on this project is in the form of two papers. The first paper, Somerville (2003), describes the magnitude scaling of the near fault rupture directivity pulse in near fault ground motions. It presents equations relating the period of the fault-normal component of the forward rupture directivity velocity pulse to the earthquake magnitude, and a model for the acceleration response spectra of near-fault fault-normal ground motions that includes the magnitude dependence of period of the response spectral peak. This paper is a revised version of a presentation made at the International Workshop on the Quantitative Prediction of Strong-Motion and the Physics of Earthquake Sources, October 23-25, 2000, Tsukuba, Japan.

The second paper, Somerville (2002), describes the characterization of near fault ground motion for engineering design, including the effects of the rupture directivity pulse and permanent ground displacements. Near-fault ground motions are different from ordinary ground motions in that they often contain strong coherent dynamic long period pulses and permanent ground displacements. The dynamic motions are dominated by a large long period pulse of motion that occurs on the horizontal component perpendicular to the strike of the fault, caused by rupture directivity effects. The static ground displacements in near-fault ground motions are caused by the relative movement of the two sides of the fault on which the earthquake occurs. These displacements are

discontinuous across a fault having surface rupture, and can subject a bridge crossing a fault to significant differential displacements. The static ground displacements occur at about the same time as the large dynamic motions, indicating that the static and dynamic displacements need to be treated as coincident loads.

REFERENCES

Somerville, P.G. (2003). Magnitude scaling of the near fault rupture directivity pulse. Physics of the Earth and Planetary Interiors, in press.

Somerville, P.G. (2002). Characterizing near fault ground motion for the design and evaluation of bridges. Proceedings of the Third National Conference and Workshop on Bridges and Highways, Portland, Oregon, April 29 – May 1, 2002.

MAGNITUDE SCALING OF THE NEAR FAULT RUPTURE DIRECTIVITY PULSE

Paul G. Somerville
URS Corporation, 566 El Dorado Street, Pasadena, CA 91101

Abstract

Current ground motion models all assume monotonically increasing spectral amplitude at all periods with increasing magnitude. However, near fault recordings from recent earthquakes confirm that the near-fault fault-normal forward rupture directivity velocity pulse is a narrow band pulse whose period increases with magnitude. This magnitude dependence of the period of the near fault pulse is expected from theory, because the period of the pulse is related to source parameters such as the rise time (duration of slip at a point on the fault) and the fault dimensions, which generally increase with magnitude. This magnitude dependence of the pulse period causes the response spectrum to have a peak whose period increases with magnitude, such that the near-fault ground motions from smaller earthquakes may exceed those of larger earthquakes at intermediate periods (around 1 second). This paper presents preliminary equations relating the period of the fault-normal component of the forward rupture directivity velocity pulse to the earthquake magnitude, and a preliminary model for the acceleration response spectra of near-fault fault-normal ground motions that includes the magnitude dependence of period of the response spectral peak.

Rupture Directivity Effects in Strong Ground Motion

An earthquake is a shear dislocation that begins at a point on a fault and spreads at a velocity that is almost as large as the shear wave velocity. The propagation of fault rupture toward a site at a velocity close to the shear wave velocity causes most of the seismic energy from the rupture to arrive in a single large pulse of motion that occurs at the beginning of the record (Archuleta and Hartzell, 1984; Somerville et al., 1997). This pulse of motion represents the cumulative effect of almost all of the seismic radiation from the fault. The radiation pattern of the shear dislocation on the fault causes this large pulse of motion to be oriented in the direction perpendicular to the fault, causing the strike-normal ground motions to be larger than the strike-parallel ground motions at periods longer than about 0.5 seconds. To accurately characterize near fault ground motions, it is therefore necessary to specify separate response spectra and time histories for the fault normal and fault parallel components of ground motion.

Forward rupture directivity effects occur when two conditions are met: the rupture front propagates toward the site, and the direction of slip on the fault is aligned with the site. The conditions for generating forward rupture directivity effects are readily met in strike-slip faulting, where the rupture propagates horizontally along strike either unilaterally or bilaterally, and the fault slip direction is oriented horizontally in the direction along the strike of the fault. However, not all near-fault locations experience

forward rupture directivity effects in a given event. Backward directivity effects, which occur when the rupture propagates away from the site, give rise to the opposite effect: long duration motions having low amplitudes at long periods.

The conditions required for forward directivity are also met in dip slip faulting. The alignment of both the rupture direction and the slip direction updip on the fault plane produces rupture directivity effects at sites located around the surface exposure of the fault (or its updip projection if it does not break the surface). Unlike the case for strike-slip faulting, where forward rupture directivity effects occur at all locations along the fault away from the hypocenter, dip slip faulting produces directivity effects on the ground surface that are most concentrated in a limited region updip from the hypocenter. For this reason, rupture directivity effects in the 1999 Chi-Chi earthquake were confined to stations such as Tsaotun (TCU075) and Mingchien (TCU129), which are located updip from the hypocenter along the southern part of the fault rupture.

Broadband Directivity Model

A model that can be used to modify conventional ground motion attenuation relations to account for the amplitude and duration effects of rupture directivity was developed by Somerville et al. (1997). This model was modified by Abrahamson (2000) to incorporate a directivity saturation effect and to taper it at small magnitudes and large distances. In the near-fault rupture directivity model of Somerville et al. (1997), as modified by Abrahamson (1998), amplitude variations due to rupture directivity depend on two geometrical parameters. First, the smaller the angle between the direction of rupture propagation and the direction of waves travelling from the fault to the site, the larger the amplitude. Second, the larger the fraction of the fault rupture surface that lies between the hypocenter and the site, up to limit of 40% of the fault length, the larger the amplitude. Abrahamson demonstrated that incorporation of the modified model in a probabilistic seismic hazard calculation results in an increase of about 30% in the spectral acceleration at a period of 3 seconds for an annual probability of 1/1,500 at a site near a large active fault.

Magnitude Scaling of Response Spectra of Near Fault Ground Motions

Strong motion recordings of the recent large earthquakes in Turkey and Taiwan confirm that the near fault pulse is a narrow band pulse whose period increases with magnitude (Figure 1). The recent earthquakes also have surprisingly weak ground motions at short and intermediate periods (0.1 to 3.0 seconds), weaker than those of smaller (magnitude 6 ¾ - 7.0) earthquakes. These observations require reevaluation of the magnitude scaling in current models of near fault ground motions and in current source scaling relations (Somerville et al., 1999).

On the left side of Figure 1, rupture directivity pulses of earthquakes in the magnitude range of 6.7 to 7 are compared with pulses from earthquakes in the magnitude range of 7.2 to 7.6. The narrow band nature of these pulses causes their elastic response spectra to have peaks, as shown on the right side of Figure 1. The fault normal components (which contain the directivity pulse) are shown as solid lines, and the fault

parallel components, which as expected are much smaller at long periods, are shown by long dashed lines. The 1994 UBC spectrum for soil site conditions is used as a reference model for comparison. The spectra for the large earthquakes (right column) are compatible with the UBC code spectrum in the intermediate period range, between 0.5 and 2.5 seconds, but have a bump at a period of about 4 seconds where they significantly exceed the UBC code spectrum. The spectra of the smaller earthquakes (left column) are very different from those of the larger earthquakes. Their spectra are much larger than the UBC code spectrum in the intermediate period range of 0.5 - 2.5 sec, but are similar to the UBC spectrum at longer periods.

These features are seen even more clearly in Figures 2 and 3, which show the velocity and displacement response spectra of the same time histories. The magnitude scaling exhibited in the data in Figures 1 through 3 is contrary to all current models of earthquake source spectral scaling and ground motion spectral scaling with magnitude, including Somerville et al. (1997), which assume that spectral amplitudes increase monotonically at all periods. However, these magnitude scaling features are the natural consequence of the narrow band character of the forward rupture directivity pulse. The period of the near fault pulse is related to source parameters such as the rise time (duration of slip at a point on the fault) and the fault dimensions, which generally increase with magnitude. Near fault ground motions cannot be adequately described by uniform scaling of a fixed response spectral shape, because the shape of the intermediate and long period part of the response changes as the level of the spectrum increases and as the magnitude increases.

Relationships between Pulse Period and Magnitude

Equations relating the period and amplitude of the fault-normal forward rupture directivity velocity pulse to earthquake magnitude and distance were developed by Somerville (1998), Somerville et al. (2000) and Alavi and Krawinkler (2000). The recordings used were mostly within 10 km of the fault, and the period was assumed to be independent of the distance from the fault. We have updated the relationship between velocity pulse period and magnitude using data from the 1999 Chi-Chi, Taiwan and Kocaeli, Turkey earthquakes. Separate relationships were developed for near fault recordings on rock and soil sites. These relationships use the period T_{Dir} of the largest cycle of the fault normal velocity waveform recorded at stations near the fault that experience forward rupture directivity. These empirical relationships are defined only for full forward rupture directivity conditions, and are not defined for the full range of angles and rupture distances that are included in the Somerville et al. (1997) response spectral model for rupture directivity effects.

The data for rock are consistent with a self-similar scaling relationship in which the period of the pulse T_{Dir} increases in proportion to the fault length. This is consistent with the self-similar nature of the source scaling relations found by Somerville et al. (1999). The relationship derived from the data listed in Table 1 and shown at the top of Figure 4 is:

$$\log10\ T_{Dir} = -3.17 + 0.5\ M_W$$

The relationship for soil is allowed to depart from self-similarity, in order to accommodate non-linear effects (Rodriguez-Marek, 2000). The effect of the soil layer is generally to increase both the peak velocity and the period of the input rock motion. The amount of the increase depends on the level of the input ground motion, and the thickness and physical properties of the soil layer. The relationship derived from the data listed in Table 2 and shown at the bottom of Figure 4 is:

$$\text{Log10 } T_{Dir} = -2.02 + 0.346\ M_W$$

These linear relationships for rock and soil intersect at $M_W = 7.4$. It is expected that the relationship for soil is actually curved, and merges with the rock relationship for magnitudes larger than 7.4, rather than having lower values of T_{Dir} than for rock at magnitudes larger than 7.4.

Narrow Band Rupture Directivity Model

The response spectral characteristics of velocity pulses whose periods follow the magnitude scaling characteristics described above are illustrated in Figure 5. Simple triangular velocity pulses that follow the relation for rock are shown on the left side, and the corresponding elastic acceleration and velocity response spectra are at the center and right. The elastic response spectra have peaks that are related to the period of the pulse. For spectral acceleration, the period of the peak is about 0.75 times the period of the velocity pulse, and for spectral velocity, the peak is at about 0.85 times the period of the pulse. Because of these peaks, the response spectra do not increase monotonically with magnitude at all periods, as is the case in conventional ground motion models. Instead, the response spectra for smaller earthquakes are stronger than the response spectra of larger earthquakes in some period ranges. These features are similar to those seen in the data shown in Figures 1 through 3.

We have derived preliminary response spectral models that include the magnitude dependence of the period of the rupture directivity pulse, derived from the relations between pulse period and magnitude given above. This response spectral model is for the horizontal fault normal component under maximum rupture directivity conditions (X cos theta = 1 in Somerville et al., 1997). To generate the spectrum, a conventional acceleration response spectrum, which is assumed to represent the fault parallel component, is scaled by a cosine-shaped function centered at a period equal to 0.75 times the value of T_{Dir} of the velocity pulse for a given magnitude M_w from the equation given above. The peak amplitude of the scaling function is 2 (with a standard error of 0.4 natural log units), and the width is about a factor of 1.5 on either side of T_{Dir}. The average horizontal component is obtained by using a scaling function with a peak amplitude of the square root of 2.

In Figure 6, we compare the response spectra for rock and soil predicted by this model with the standard model of Abrahamson and Silva (1997), which does not explicitly include directivity effects, and the broadband model of Somerville et al. (1997), whose directivity effects are based on the monotonic increase of ground motion

amplitudes with magnitude at all response spectral periods. The new models produce larger response spectra in the period range of about 0.5 to 2 seconds for earthquakes smaller than M_W 7.5, and smaller response spectra at all periods for earthquakes larger than M_W 7.5, compared with the Somerville et al. (1997) model.

Ground Motions from Surface and Subsurface Faulting

The recent large earthquakes in Turkey and Taiwan, which caused large surface ruptures, have surprisingly weak ground motions at short and intermediate periods. These new observations are consistent with our finding from previous earthquakes that the strong ground motions of earthquakes that produce surface faulting are weaker than the ground motions of events whose rupture is confined to the subsurface. The rupture of the 1989 Loma Prieta and 1994 Northridge earthquakes stopped at depths of several km below the surface. Although there was some surface faulting on Awaji Island during the 1995 Kobe earthquake, the strong motion recordings of the Kobe event were dominated by subsurface faulting on the Suwa and Sumayama faults. Thus all of the earthquakes in the magnitude range of 6.7 – 7.0 shown in Figures 1 though 3 are characterized by subsurface faulting, while all of the earthquakes in the magnitude range of 7.2 to 7.6 are characterized by large amounts of surface faulting. Consequently, some of the differences seen in these figures may be attributable not only to magnitude effects, but to the effects of buried faulting. Indeed, at short and intermediate periods, the ground motions from earthquakes that produce large surface rupture appear to be systematically weaker than those whose rupture is confined to the subsurface, although current empirical ground motion models do not distinguish between these different categories of earthquakes.

Current ground motion models do not distinguish between surface and subsurface faulting earthquakes, but instead describe the average ground motion properties of the two categories combined. The Abrahamson and Silva (1997) model was derived from strong motion recordings of shallow crustal earthquakes using the random effects method (Abrahamson and Youngs, 1992). The random effects method separates event terms from site terms using maximum likelihood. The event term represents the difference between the ground motions of an individual earthquake and those of the average earthquake as defined by the ground motion model for a given earthquake magnitude, closest distance, and site category.

The event terms for a set of surface rupture earthquakes are shown at the top and center of Figure 7, and for a set of subsurface rupture earthquakes at the bottom. The zero line represents the Abrahamson and Silva (1997) model, and lines above the zero line indicate that the event's ground motions on average exceed the model. The event terms of the 1999 Turkey and Taiwan events are represented by their residuals from the model. At periods between 0.3 and 3.0 seconds, the ground motions from earthquakes that produce large surface rupture are only about one-half as strong as those in which rupture is confined to the subsurface. This preliminary result needs to be verified using a more complete data set.

Conclusions

Strong motion recordings of the recent Taiwan and Turkey earthquakes confirm that the near fault rupture directivity pulse is a narrow band pulse whose period increases with magnitude. The period of the near fault pulse is related to source parameters such as the rise time (duration of slip at a point on the fault) and the fault dimensions, which generally increase with magnitude. Near fault ground motions containing forward rupture directivity may be simple enough to be represented by simple time domain pulses. We present preliminary equations relating the period of the fault-normal component of the forward rupture directivity velocity pulse to the earthquake magnitude for both rock and soil sites.

The narrow band nature of these pulses causes their elastic response spectra to have peaks whose period increases with magnitude. The elastic spectra of near-fault recordings of earthquakes with magnitudes 6.75 to 7.0 are much stronger than those of the larger earthquakes (magnitudes 7.25 to 7.5) in the intermediate period range of 0.5 - 2.5 sec, but are weaker at longer periods. This magnitude scaling is contrary to current models of earthquake source spectral scaling and ground motion spectral scaling with magnitude, which assume that spectral amplitudes increase monotonically at all periods. We present a preliminary model for the acceleration response spectra of near-fault fault-normal ground motions that includes the magnitude dependence of the period of the peak in the response spectrum for both rock and soil sites.

At short and intermediate periods, the ground motions from earthquakes that produce large surface rupture appear to be systematically weaker than ground motions from earthquakes whose rupture is confined to the subsurface. In particular, the recent Turkey and Taiwan earthquakes have surprisingly weak ground motions at short and intermediate periods (0.1 to 3.0 seconds), about 40% weaker than those of current empirical ground motion models.

References

Abrahamson, N.A., 2000. Effects of rupture directivity on probabilistic seismic hazard analysis. Proceedings of the 6th International Conference on Seismic Zonation, Palm Springs, Earthquake Engineering Research Institute.

Abrahamson. N.A. and W.J. Silva, 1997. Empirical response spectral attenuation relations for shallow crustal earthquakes. Seismological Research Letters, 68: 94-127.

Alavi, B. and H. Krawinkler, 2000. Design considerations for near-fault ground motions. Proceedings of the U.S. – Japan Workshop on the Effects of Near-Fault Earthquake Shaking, San Francisco, March 20-21.

Archuleta, R. J. and S. H. Hartzell, 1981. Effects of fault finiteness on near-source ground motion. Bull. Seismol. Soc. Am., 71: 939-957.

Rodriguez-Marek, A., 2000. Near fault seismic site response. Ph.D. Thesis, Civil Engineering, University of California, Berkeley, 451 pp.

Somerville, P.G., H. Krawinkler and B. Alavi, 2000. Development of improved ground motion representation and design procedures for near-fault ground motions. Final Report to CSMIP Data Utilization Program, Contract No. 1097-601.

Somerville, P.G., K. Irikura, R, Graves, S. Sawada, D. Wald, N. Abrahamson, Y. Iwasaki, T. Kagawa, N. Smith and A. Kowada, 1999. Characterizing crustal earthquake slip models for the prediction of strong ground motion. Seismological Research Letters, 70: 59-80.

Somerville, P.G. (1998). Development of an improved representation of near fault ground motions. Proc. of the SMIP98 Seminar on Utilization of Strong Ground Motion Data, p 1-20.

Somerville, P.G., N.F. Smith, R.W. Graves, and N.A. Abrahamson (1997). Modification of empirical strong ground motion attenuation relations to include the amplitude and duration effects of rupture directivity. Seismological Research Letters, 68: 199-222.

Table 1. Period of the Forward Rupture Directivity Pulse Recorded on Rock

Earthquake	Magnitude (Mw)	Recording Station	Closest Distance (km)	Peak Velocity (cm/sec)	Period of Vel. Pulse (sec)
Kocaeli	7.4	Gebze	18.2	37.68	4.7
Landers	7.3	Lucerne	1.1	136.04	5.0
Loma Prieta	7.0	Los Gatos Pres. Center	3.5	103.91	2.8
		Lexington Dam	6.3	118.23	2.4
Kobe	6.9	JMA	0.6	104.29	1.55
		Kobe Univ.	1.0	49.08	1.6
Northridge	6.7	Jensen Generator	6.4	31.76	1.2
		Rinaldi	7.1	175.0	1.28
		LA Dam	6.8	79.73	1.24
		Pacoima Dam Abut.	7.8	107.90	0.9
San Fernando	6.6	Pacoima Dam Abut.	3.5	114.53	1.44
Morgan Hill	6.2	Anderson Dam	3.5	26.71	0.79
		Coyote Lake Dam	0.5	66.13	0.92
		Gilroy #6	11.8	36.40	1.1
Parkfield	6.1	Temblor	4.4	13.0	0.6

Table 2. Period of the Forward Rupture Directivity Pulse Recorded on Soil

Earthquake	Magnitude (Mw)	Recording Station	Closest Distance (km)	Peak Velocity (cm/sec)	Period of Vel. Pulse (sec)
Chi-chi	7.6	Tsaotun	5.9	116.0	4.3
Kocaeli	7.4	Yarimca	5.0	96.0	4.7
Loma Prieta	7.0	Gilroy #3	14.4	49.3	1.5
Kobe	6.9	Takatori	2.0	175.0	1.65
		Port Is downhole base	2.5	84.3	2.25
Northridge	6.7	Olive View Hospital	6.4	122.2	2.24
		Sylmar Converter	6.2	131.1	2.6
		Sylmar Converter E	6.1	116.3	2.6
		Newhall Fire Station	7.1	118.2	2.2
		Newhall Pico Cyn	7.2	108.9	2.1
		Jensen Filtration Plant	6.2	101.1	1.4
Erzincan	6.7	Erzincan	2.0	120.2	2.5

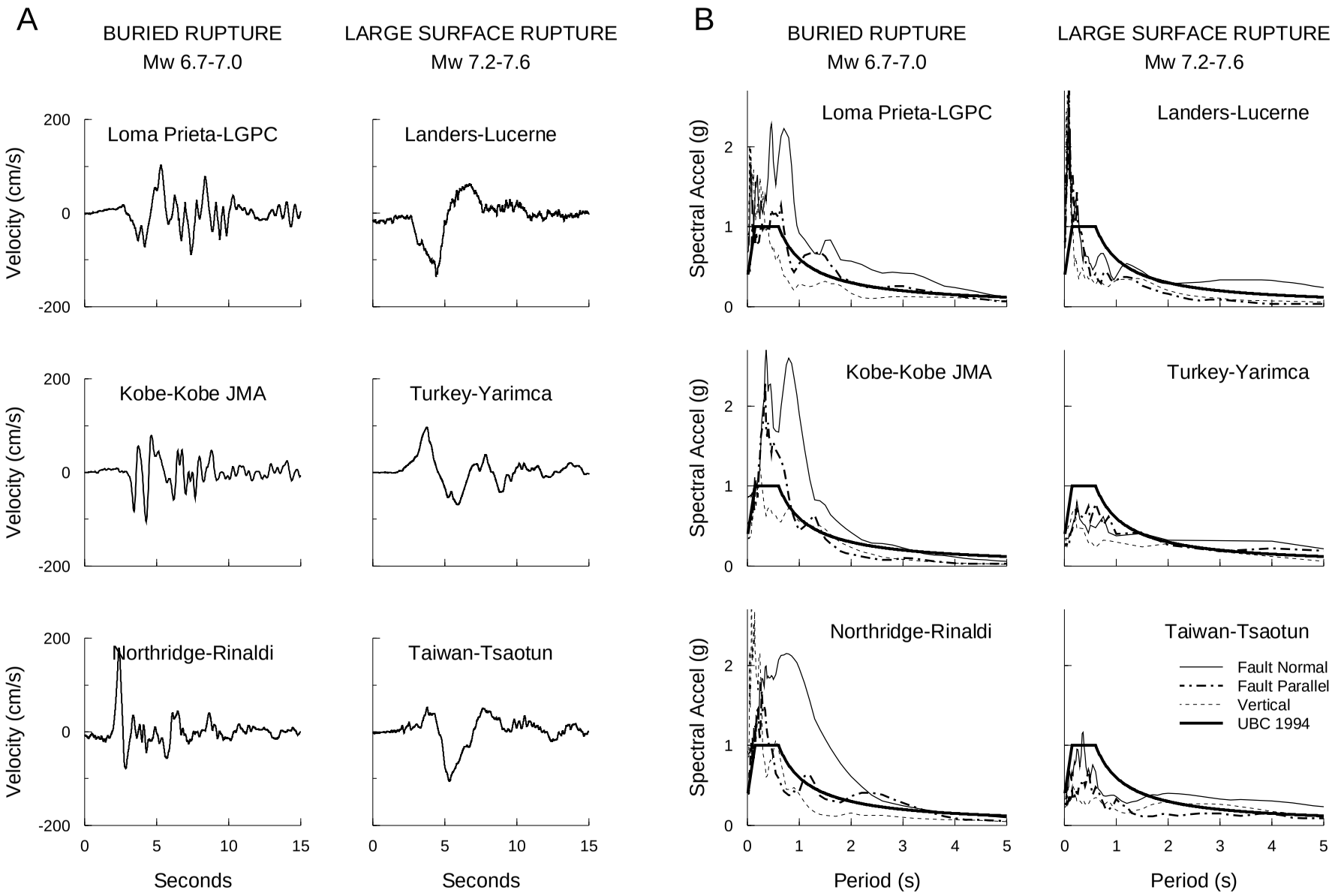

Figure 1. A: Fault-normal velocity pulses recorded near three moderate magnitude earthquakes (left column) and three large magnitude earthquakes (right column), shown on the same scales. B: Corresponding acceleration response spectra, with 1994 UBC code spectrum shown for reference.

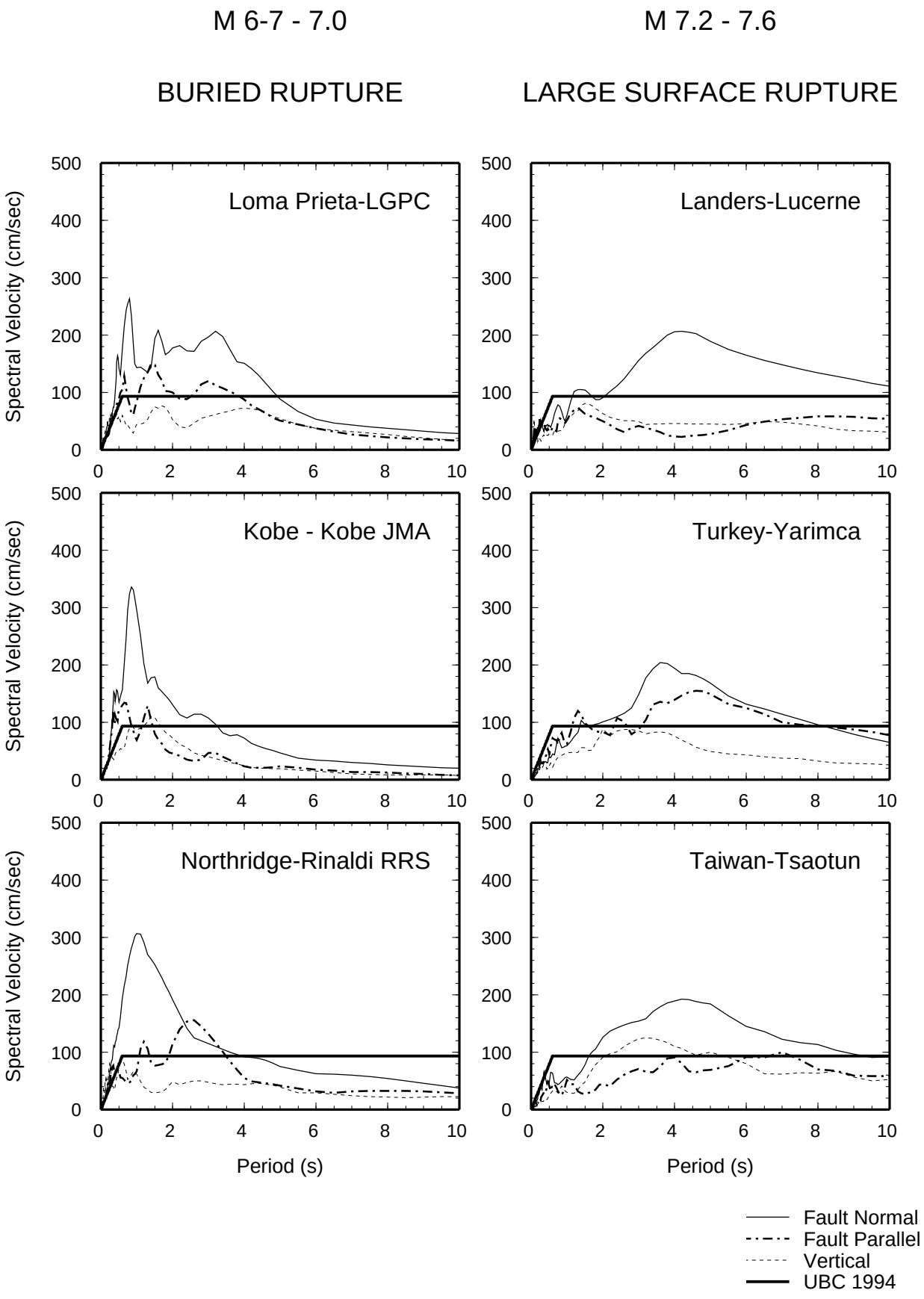

Figure 2. Spectral velocity of fault-normal pulses of moderate (left) and large (right) earthquakes.

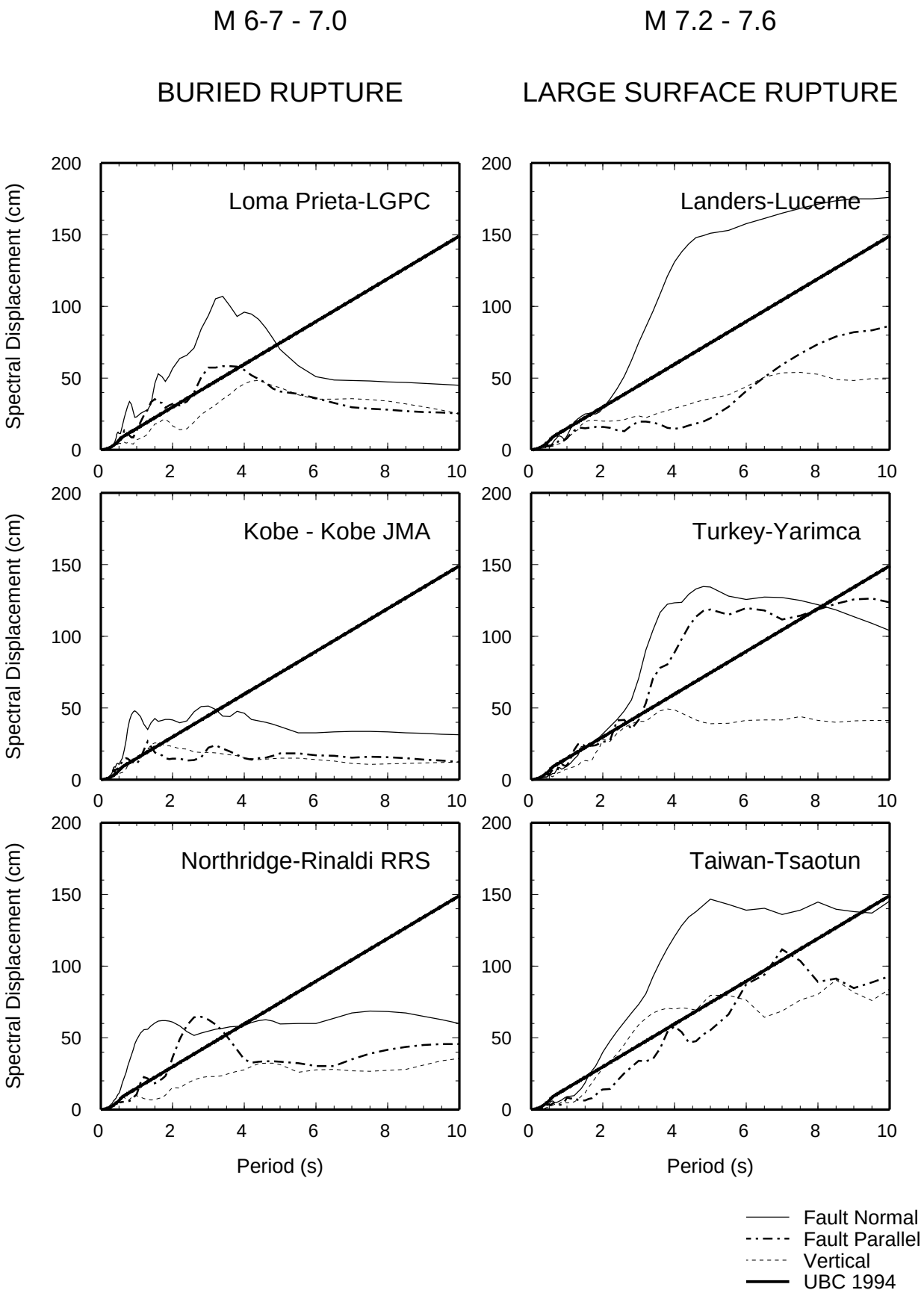

Figure 3. Spectral displacement of fault-normal pulses of moderate (left) and large (right) earthquakes.

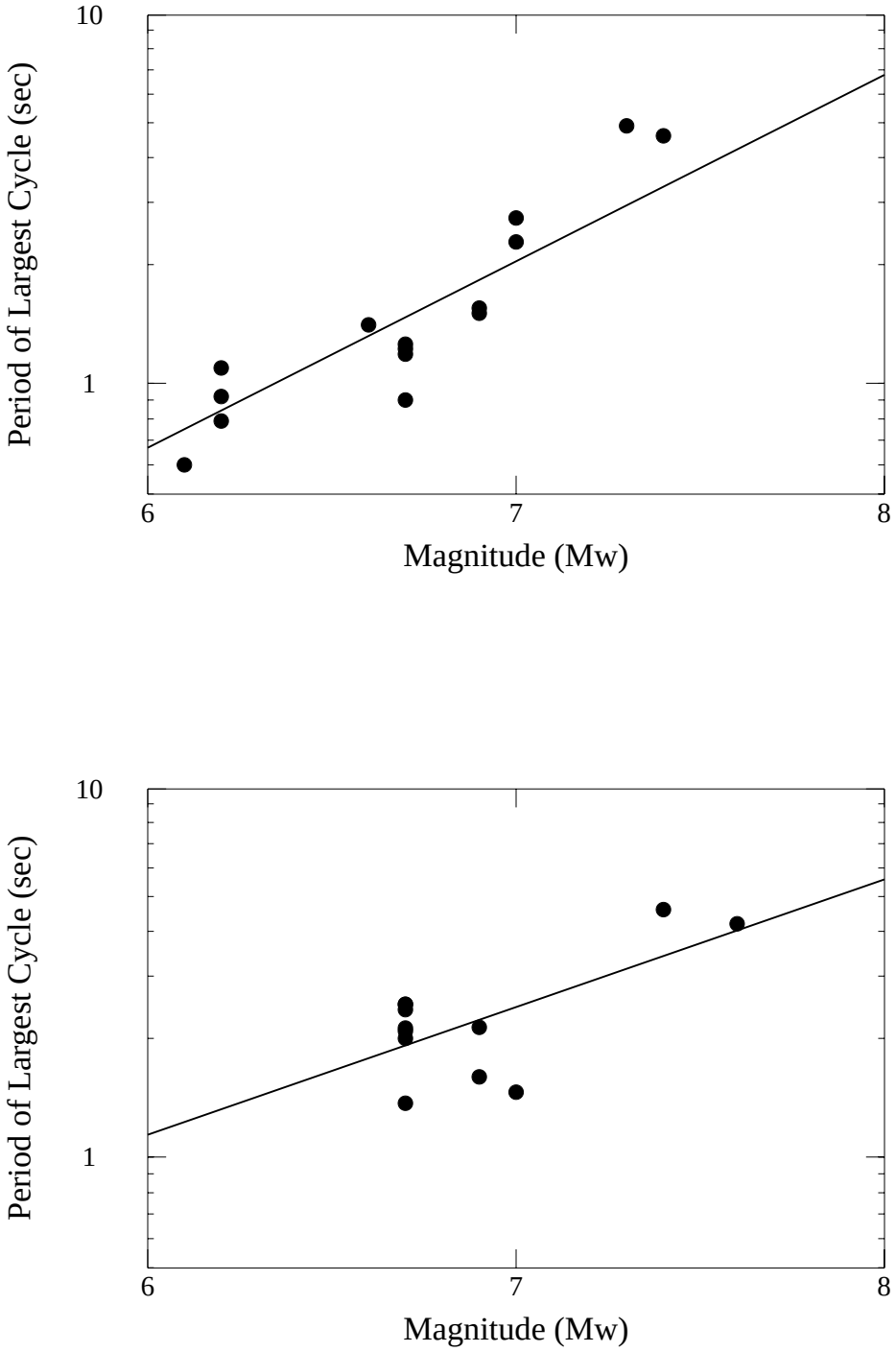

Figure 4. Mw scaling of the period of the forward rupture directivity velocity pulse on rock (top) and soil (bottom).

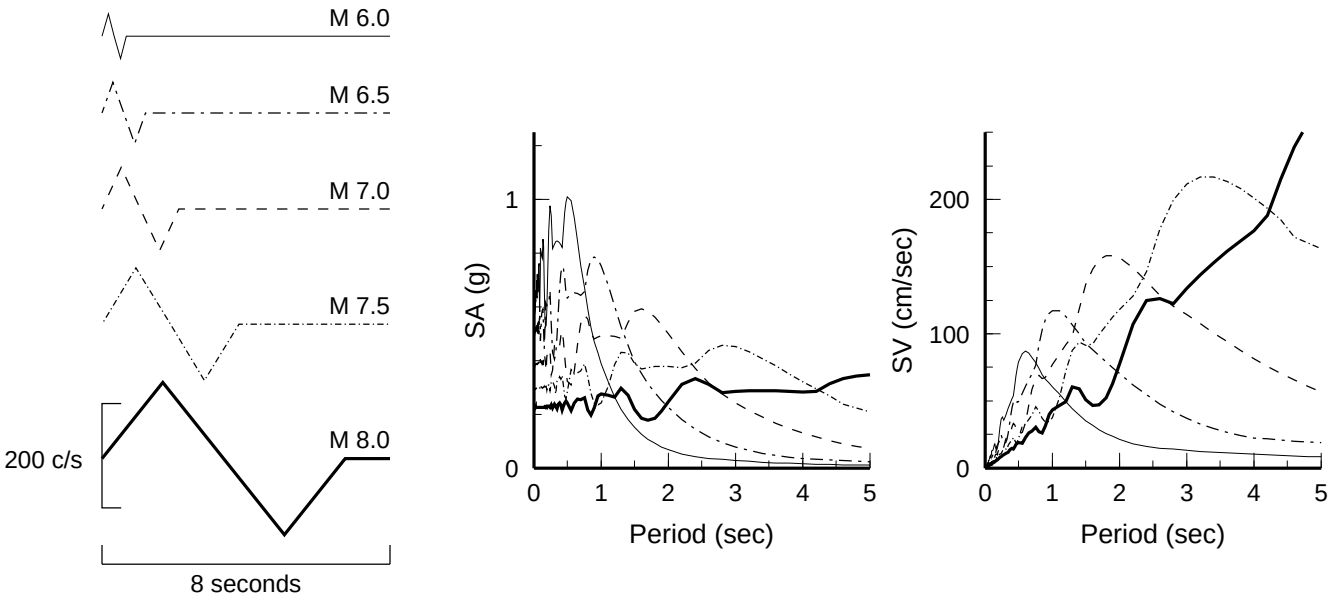

Figure 5. Magnitude scaling of simple velocity pulses representing near fault ground motions (left), and their acceleration (center) and velocity (right) response spectra.

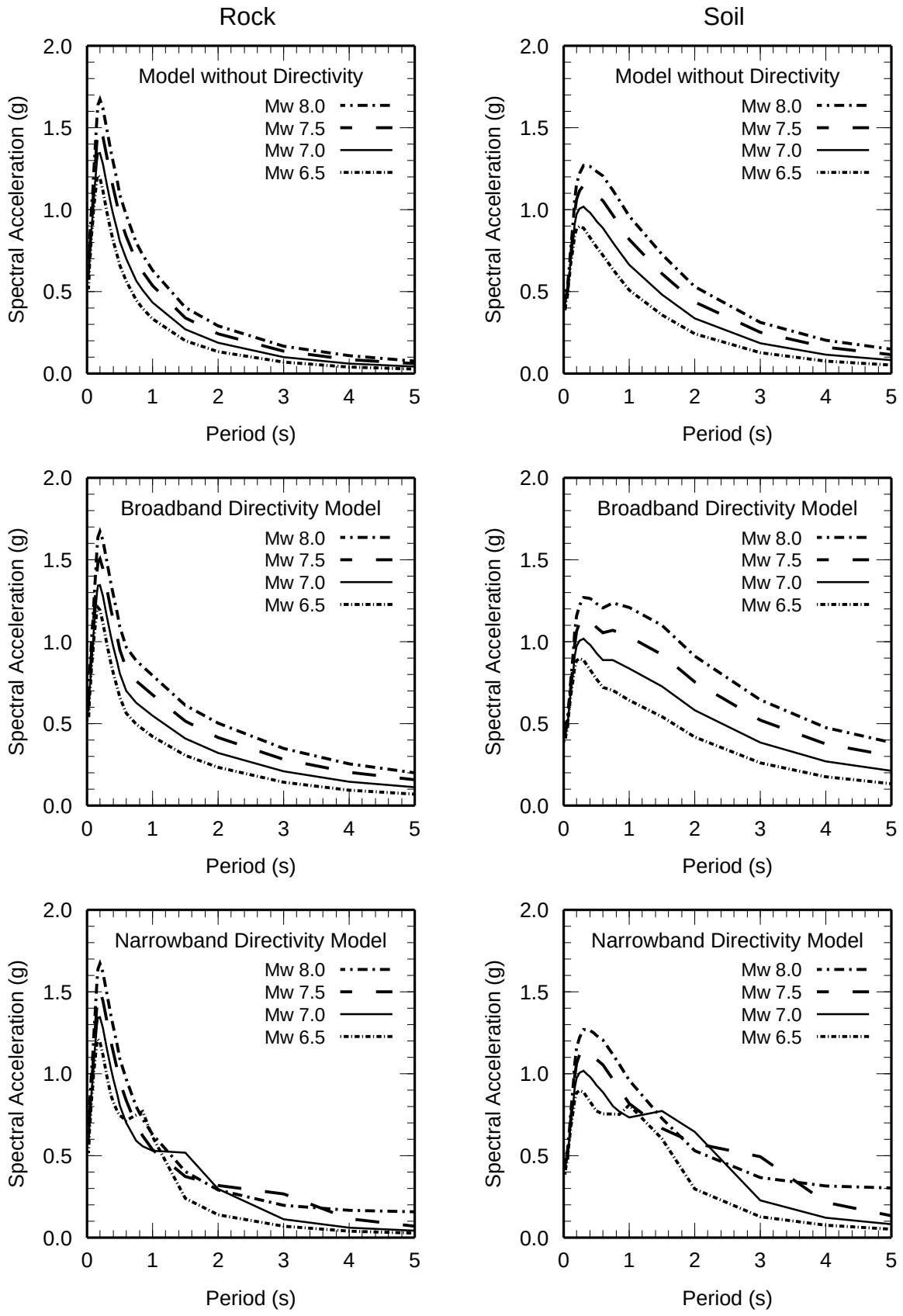

Figure 6. Near fault response spectral model, strike-slip, 5km for rock sites (left) and soil sites (right). Top: model without directivity (Abrahamson and Silva, 1997). Middle: Broadband directivity model (Somerville et al., 1997). Bottom: Narrow band directivity model (this study).

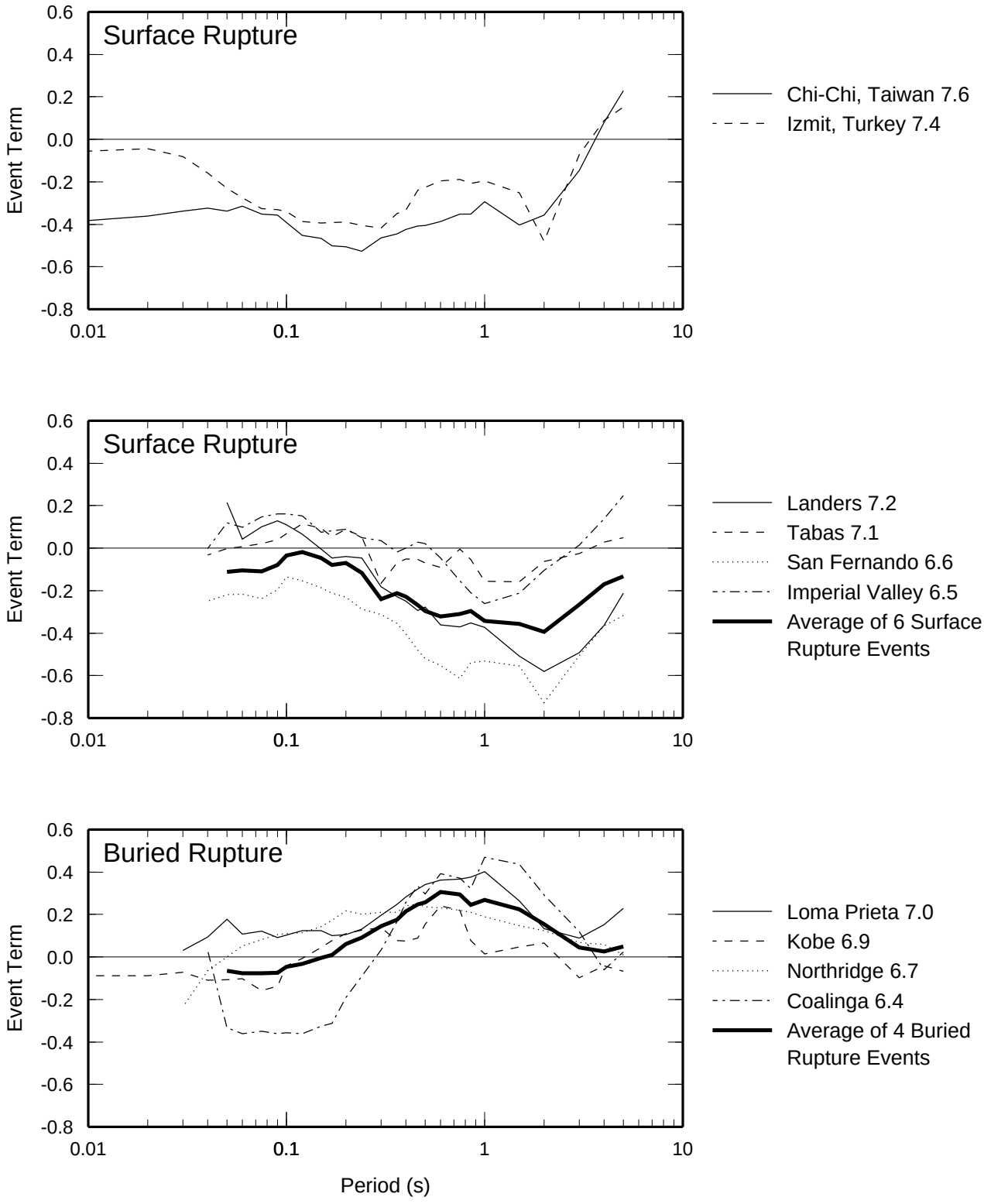

Figure 7. Comparison of the response spectral amplitude of individual earthquakes, averaged over recording sites, with the amplitude of the average earthquake as represented by the model of Abrahamson and Silva (1997), shown as the zero line, which accounts for the magnitude, closest distance and site category. The event terms (residuals) are shown as the natural logarithm of the event/model ratio: +0.2 indicates event exceeding the model by a factor of 1.22, and -0.2 indicates event at 0.82 of model value.

Third National Seismic Conference & Workshop on Bridges & Highways
Portland, Oregon, April 29 – May 1, 2002

Characterizing Near Fault Ground Motion For The Design And Evaluation Of Bridges

Paul Somerville

ABSTRACT

Near-fault ground motions are different from ordinary ground motions in that they often contain strong coherent dynamic long period pulses and permanent ground displacements. The dynamic motions are dominated by a large long period pulse of motion that occurs on the horizontal component perpendicular to the strike of the fault, caused by rupture directivity effects. Near fault recordings from recent earthquakes indicate that this pulse is a narrow band pulse whose period increases with magnitude, as expected from theory. This magnitude dependence of the pulse period causes the response spectrum to have a peak whose period increases with magnitude, such that the near-fault ground motions from moderate magnitude earthquakes may exceed those of larger earthquakes at intermediate periods (around 1 second). The static ground displacements in near-fault ground motions are caused by the relative movement of the two sides of the fault on which the earthquake occurs. These displacements are discontinuous across a fault having surface rupture, and can subject a bridge crossing a fault to significant differential displacements. The static ground displacements occur at about the same time as the large dynamic motions, indicating that the static and dynamic displacements need to be treated as coincident loads.

At the FHWA/NCEER Workshop on the National Representation of Seismic Ground Motion for New and Existing Highway Facilities held in San Francisco on May 29-30, 1997, a consensus was reached that the response spectrum alone is not an adequate representation of near-fault ground motion characteristics, because it does not adequately represent the demand for a high rate of energy absorption presented by near-fault pulses. This is especially true for high ground motion levels that drive structures into the non-linear range, invalidating the linear elastic assumption on which the elastic response spectrum is based. To fully portray the response of structures to near-fault ground motions, nonlinear time history analysis may be required. Fortunately, near fault ground motions containing forward rupture directivity may be simple enough to be represented by simple time domain pulses, thus simplifying the specification of ground motion time histories for use in structural response analyses. Preliminary equations relating the period of the pulse to the earthquake magnitude, and the effective velocity of the pulse to the earthquake magnitude and distance, have been developed. The directivity pulse can be combined with the static fault displacement to provide a complete description on near-fault ground motions. The effect of the simultaneous dynamic and static ground motions on the response of a bridge should be analyzed using time histories that include both types of motion.

The probabilistic approach to seismic hazard analysis has an important advantage over the deterministic approach in that it takes into account the degree of activity of the faults that contribute to the hazard, providing explicit estimates of the likelihood of occurrence (or return period) of the hazard level that is specified in the design ground motions.

Paul Somerville, Principal Seismologist, URS Corp., 566 El Dorado St., Pasadena, CA 91101

INTRODUCTION

An earthquake occurs when elastic strain that has gradually accumulated across a fault is suddenly released in the process of elastic rebound. The elastic energy stored on either side of the fault drives the motion on the fault. The elastic rebound generates dynamic strong ground motions that last for a few seconds to a few minutes, constituting a primary seismic hazard. The elastic rebound also generates static deformation of the ground. The static deformation of the ground consists of a discontinuity in displacement on the fault itself, and a gradual decrease in this displacement away from the fault on either side of the fault. If there is surface faulting, the static displacements are discontinuous across the fault at the ground surface, constituting a primary seismic hazard. Even if the fault does not break the surface, there is static deformation of the ground surface due to subsurface faulting.

Strong ground motions recorded on digital accelerographs in recent earthquakes, including the 1985 Michoacan, Mexico, 1999 Chi-chi, Taiwan and 1999 Kocaeli, Turkey earthquakes, contain both dynamic ground motions and static ground displacements. Figure 1 shows the strong motion recording of the strike-slip Kocaeli earthquake at Yarimca. The static displacement of the ground is about 2 meters in the east-west direction, parallel to the strike of the fault, consistent with geological and GPS data. The large dynamic ground velocity pulse is oriented north-south, in the fault normal direction. The static ground displacement is coincident in time with the largest dynamic ground velocities, as shown in Figure 1, and occurs over a time interval of several seconds. It is therefore necessary to treat the dynamic and static components of the seismic load as coincident loads.

In some earthquakes, faulting of the ground surface occurs on a distributed system of sub-parallel faults instead of occurring on a single fault trace. This distributed fault system may have a width of several tens to hundreds of meters. This does not have a significant impact on the estimation of dynamic ground motions, but can complicate the estimation of the static ground displacement field, including surface faulting. Ground shaking can cause secondary ground deformation by inducing soil liquefaction with concomitant lateral spreading, and landslides. Excluding these complications and secondary effects, the near fault ground motion hazards that influence an individual bridge support include:

- Dynamic displacements at a bridge support due to seismic waves
- Permanent displacements at a bridge support due to the static displacement field

These dynamic and static ground displacements need to be quantified in separate hazard analyses, because they are not strongly correlated, as shown below. Once they have been separately quantified, the two components of the hazard can then be combined into a single ground motion time history, like those shown in Figure 1, that contains both dynamic and static ground displacements at a bridge support.

Bridges have multiple supports and are thus also affected by differential displacements of the ground. These differential displacements may be caused by both dynamic and static ground displacements. The kinds of seismic hazards that cause differential ground displacements of bridge piers in the near fault environment include:

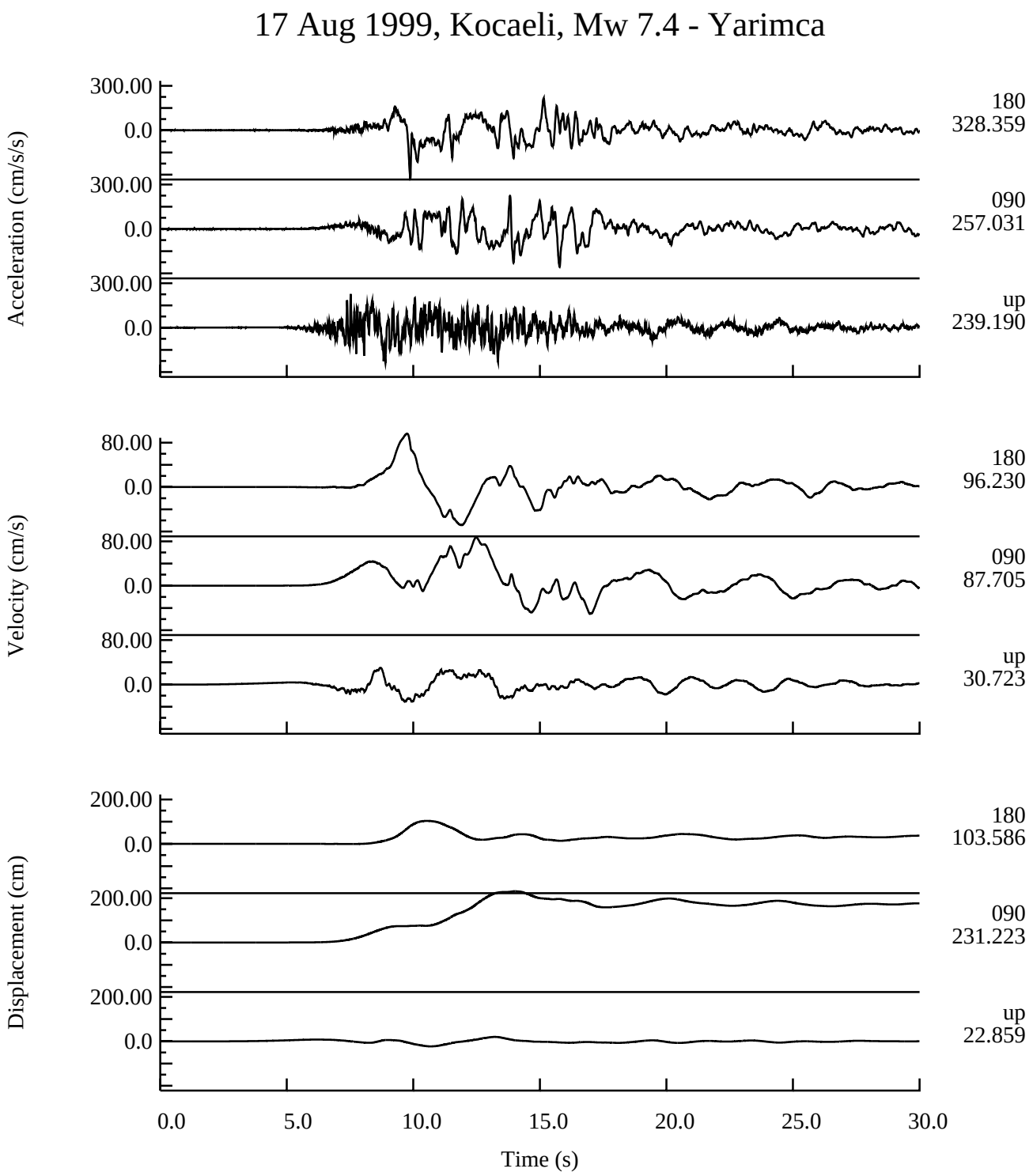

Figure 1. Strong motion recording of the south (180), east (090), and vertical (up) components of the 1999 Kocaeli, Turkey earthquake at Yarimca.

- Dynamic differential displacements between supports due to seismic waves. These include the effects of wave passage, and differences in the amplitude and phase of ground motions at multiple supports due to wave incoherence effects [1].

- Permanent differential displacements between supports due to the static displacement field. These are potentially large when surface faulting occurs between supports. Even without surface displacements between supports, differential displacements may occur due to spatial variations in the static displacement field, which may be significant near the fault.

These dynamic and static differential displacement hazards need to be quantified in separate hazard analyses. However, both components of the hazard can be specified together by suites of ground motion time histories at multiple supports that contain both dynamic and static ground displacements whose differential values between supports are consistent with the estimated differential displacement hazards.

NEAR FAULT RUPTURE DIRECTIVITY PULSE

An earthquake is a shear dislocation that begins at a point on a fault and spreads at a velocity that is almost as large as the shear wave velocity. The propagation of fault rupture toward a site at a velocity close to the shear wave velocity causes most of the seismic energy from the rupture to arrive in a single large pulse of motion that occurs at the beginning of the record [2], [3]. This pulse of motion represents the cumulative effect of almost all of the seismic radiation from the fault. The radiation pattern of the shear dislocation on the fault causes this large pulse of motion to be oriented in the direction perpendicular to the fault plane, causing the strike-normal component of ground motion to be larger than the strike-parallel component at periods longer than about 0.5 seconds. To accurately characterize near fault ground motions, it is therefore necessary to specify separate response spectra and time histories for the strike-normal and strike-parallel components of ground motion.

Forward rupture directivity effects occur when two conditions are met: the rupture front propagates toward the site, and the direction of slip on the fault is aligned with the site. The conditions for generating forward rupture directivity effects are readily met in strike-slip faulting, where the rupture propagates horizontally along strike either unilaterally or bilaterally, and the fault slip direction is oriented horizontally in the direction along the strike of the fault. However, not all near-fault locations experience forward rupture directivity effects in a given event. Backward directivity effects, which occur when the rupture propagates away from the site, give rise to the opposite effect: long duration motions having low amplitudes at long periods.

The conditions required for forward directivity are also met in dip slip faulting. The alignment of both the rupture direction and the slip direction updip on the fault plane produces rupture directivity effects at sites located around the surface exposure of the fault (or its updip projection if it does not break the surface). Unlike the case for strike- slip faulting, where forward rupture directivity effects occur at all locations along the fault away from the hypocenter, dip slip faulting produces directivity effects on the ground surface that are most concentrated in a limited region updip from the hypocenter.

ORIENTATION OF DYNAMIC AND STATIC NEAR FAULT GROUND MOTIONS

The top part of Figure 2 schematically illustrates the orientations of dynamic and static near fault ground motions. The strike-slip case is shown in map view, where the fault defines the strike direction. The rupture directivity pulse is oriented in the strike-normal direction and the static ground displacement ("fling step") is oriented parallel to the fault strike. The dip-slip case is shown in vertical cross section, where the fault defines the dip direction; the strike direction is orthogonal to the page. The rupture directivity pulse is oriented in the direction normal to the fault dip, and has components in both the vertical direction and the horizontal strike normal directions. The static ground displacement is oriented in the direction parallel to the fault dip, and has components in both the vertical direction and the horizontal strike normal direction.

The bottom part of Figure 2 schematically illustrates the partition of near fault ground motions into the dynamic ground motion, which is dominated by the rupture directivity pulse, and the static ground displacement. For a strike-slip earthquake, the rupture directivity pulse is partitioned mainly on the strike-normal component, and the static ground displacement is partitioned on the strike-parallel component. If the static ground displacement is removed from the strike-parallel component, very little dynamic motion remains. For a dip-slip earthquake, the dynamic and static displacements occur together on the strike-normal component, and there is little of either motion on the strike-parallel component. If the static ground displacement is removed from the strike-normal component, a large directivity pulse remains.

PRESERVING ORIENTATION IN THE ARCHIVING, ANALYSIS AND APPLICATION OF NEAR FAULT GROUND MOTIONS

Figures 1 and 2 demonstrate that near-fault ground velocities and displacements have orientations that are controlled by the geometry of the fault, specifically by the strike, dip, and rake angle (direction of slip) on the fault. Consequently, it is necessary to treat them as vector, rather than scalar, quantities. The simplest method or treating them as vector quantities is to partition them into strike-normal and strike-parallel components. The dynamic and static motions are distinctly different on these two components at all near-fault locations.

Accordingly, near-fault ground motion recordings should be archived in the strike-normal and strike-parallel components, as shown on the left side of Figure 3. The rotation of the two recorded components North (N) and East (E) into strike-parallel and strike-normal components SP and SN is accomplished using the following transformations:

$$SP = N \cos \phi + E \sin \phi; \quad SN = -N \sin \phi + E \cos \phi$$

where ϕ is the strike of the fault measured clockwise from North. If the recording orientation is not North and East but rotated clockwise by the angle ψ, then ϕ would be reduced by ψ.

Distinct models for the strike-normal and strike-parallel components of near-fault ground motions, derived from appropriately archived recordings and from simulations based on seismological models, are needed for seismic hazard analysis. In order to represent near-fault effects, ground motion simulations need to be based on the summation of complete Green's functions that contain near-, intermediate-, and far-field terms. This is done using the

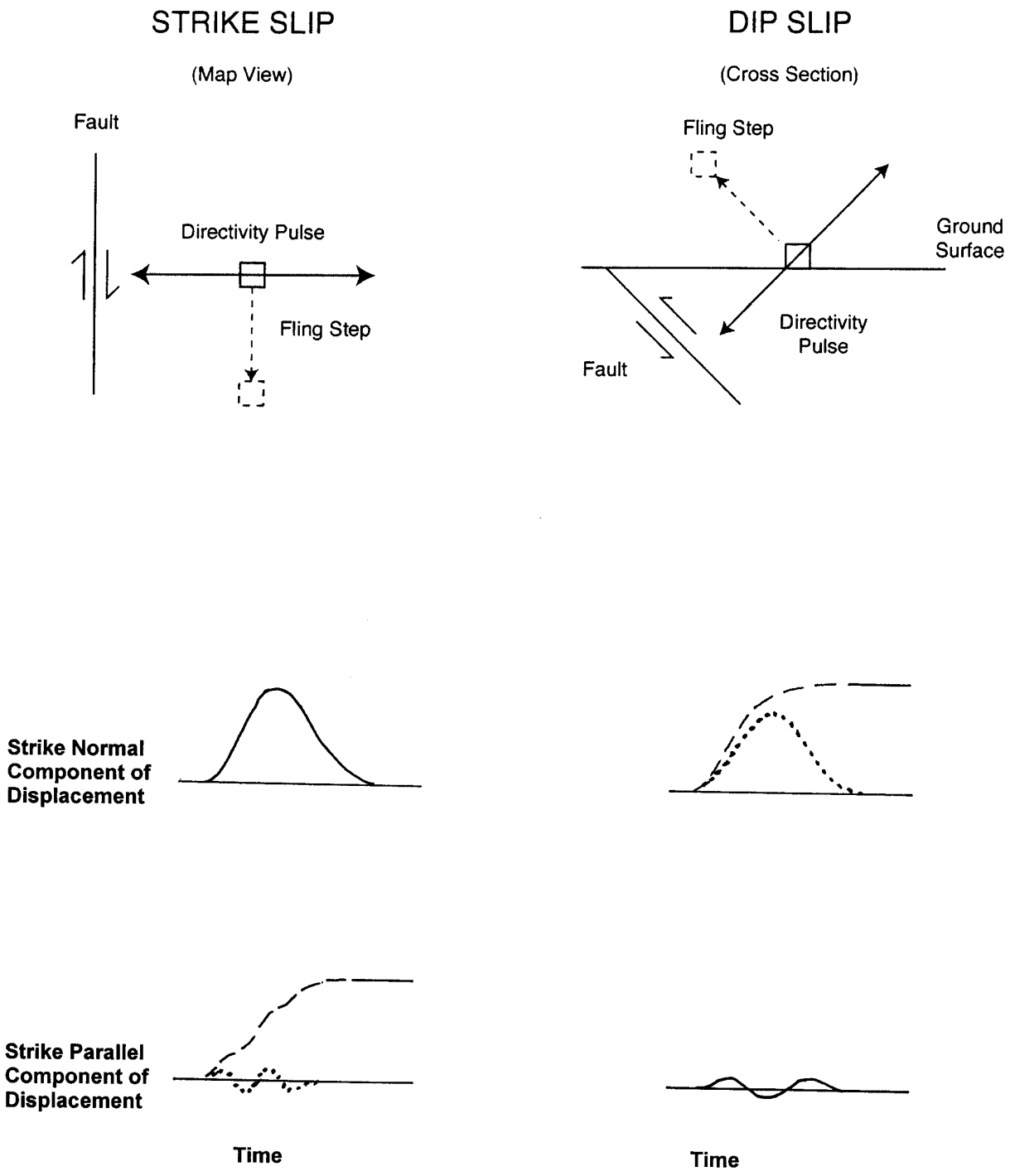

Figure 2. Top: Schematic orientation of the rupture directivity pulse and fault displacement ("fling step") for strike-slip (left) and dip-slip (right) faulting. Bottom: Schematic partition of the rupture directivity pulse and fault displacement between the strike normal and strike parallel components of ground displacement. Waveforms containing static ground displacement are shown as dashed lines; versions of these waveforms with the static displacement removed are shown as dotted lines.

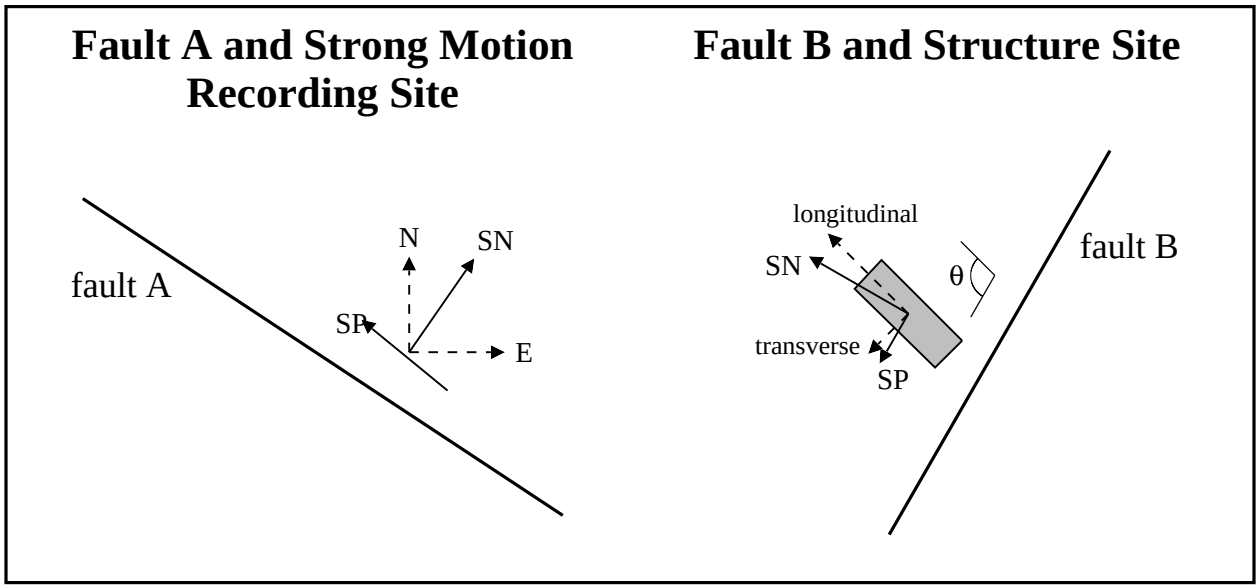

Figure 3. Archiving (left) and application (right) of strike-normal and strike-parallel components of ground motion.

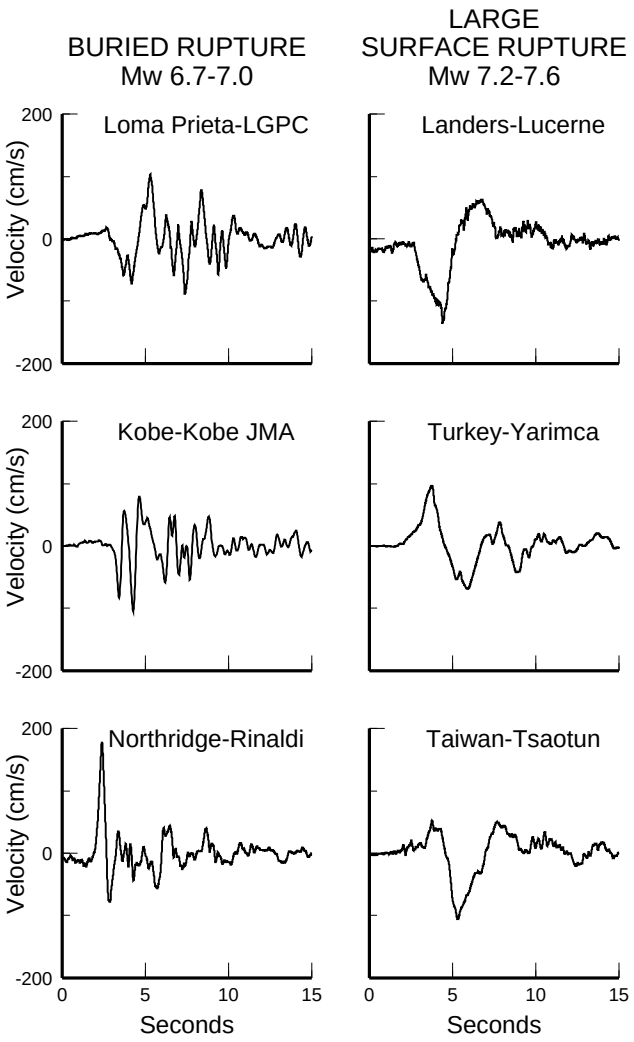

Figure 4. Fault-normal velocity pulses recorded near three moderate magnitude earthquakes (left column) and three large magnitude earthquakes (right column), shown on the same scales.

elastodynamic representation theorem, which states that the ground motion U(t) can be calculated from the convolution of the slip time function D(t) on the fault with the Green's function G(t) for the appropriate distance and depth, integrated over the fault rupture surface [4]:

$$U(t) = \sum D(t) * G(t)$$

When a near-fault ground motion time history is used for the analysis of a structure at a site, the strike-normal and strike-parallel components need to be oriented with respect to the strike of the fault that dominates the seismic hazard at the site. The strike-normal and strike-parallel components may be transformed into longitudinal and transverse components, preserving the orientation of the motions with respect to the fault strike, as illustrated on the right side of Figure 3. If the axis of the structure is aligned at some angle θ to the strike of the fault, then the longitudinal and transverse time histories can be derived from the strike-normal (SN) and strike-parallel (SP) time histories using the following transformation:

$$long = SP \cos\theta + SN \sin\theta; \quad trans = SP \sin\theta - SN \cos\theta$$

NEAR FAULT GROUND MOTION MODELS

The relationships between the dynamic and static components of near-fault ground displacements are quite complex, as illustrated in Figure 2. For example, the rupture directivity pulse and the static ground displacement occur on orthogonal components in strike-slip faulting, but on the same component in dip-slip faulting. The rupture directivity pulse can be very strong off the end of a strike-slip fault, where there is little or no static displacement. The 1989 Loma Prieta and 1994 Northridge earthquakes produced strong rupture directivity pulses even though they did not rupture the ground surface. This indicates that separate models are needed for predicting the dynamic and static components of near-fault ground displacements at a site. The separately estimated dynamic and static components of the ground motion can be combined to produce ground motion time histories representing both effects. In the following, we present models for predicting dynamic near fault ground motions. The static displacement field of earthquakes can be calculated using theoretical methods [4], and surface fault displacements can be estimated using empirical models [5].

Broadband Directivity Model

Somerville et al. [3] developed a model for near-fault ground motions that assumes monotonically increasing spectral amplitude at all periods with increasing magnitude. This model can be used to modify conventional ground motion attenuation relations to account for the amplitude and duration effects of rupture directivity. Abrahamson [6] demonstrated that incorporation of a modified version of this model in a probabilistic seismic hazard calculation results in an increase of about 30% in the spectral acceleration at a period of 3 seconds for an annual probability of 1/1,500 at a site near a large active fault.

Narrow Band Directivity Model

Strong motion recordings of the recent large earthquakes in Turkey and Taiwan indicate that the near fault pulse is a narrow band pulse whose period increases with magnitude. In Figure 4, forward rupture directivity pulses of earthquakes in the magnitude range of 6.7 to 7 are compared with pulses from earthquakes in the magnitude range of 7.2 to 7.6. The narrow band nature of

these pulses causes their elastic response spectra to have peaks, as shown in Figure 5. The fault normal components (which contain the directivity pulse) are shown as solid lines, and the fault parallel components, which are much smaller at long periods as expected, are shown by long dashed lines. The 1994 UBC spectrum for soil site conditions is used as a reference model for comparison. The spectra for the large earthquakes (right column) are compatible with the UBC code spectrum in the intermediate period range, between 0.5 and 2.5 seconds, but have a peak at a period of about 4 seconds where they significantly exceed the UBC code spectrum. The spectra of the smaller earthquakes (left column) are very different from those of the larger earthquakes. Their spectra are much larger than the UBC code spectrum in the intermediate period range of 0.5 - 2.5 sec, but are similar to the UBC spectrum at longer periods.

The recent large earthquakes in Turkey and Taiwan, which caused large surface ruptures, have surprisingly weak ground motions at short and intermediate periods. These new observations are consistent with our finding from previous earthquakes that the strong ground motions of earthquakes that produce surface faulting are weaker than the ground motions of events whose rupture is confined to the subsurface. All of the earthquakes in the magnitude range of 6.7 – 7.0 shown in Figures 4 and 5 are characterized by subsurface faulting, while all of the earthquakes in the magnitude range of 7.2 to 7.6 are characterized by large surface displacements. Consequently, some of the differences seen in these figures may be attributable not only to magnitude effects, but to the effects of buried faulting [7].

The magnitude scaling exhibited in the data in Figures 4 and 5 is contrary to all current models of earthquake source spectral scaling and ground motion spectral scaling with magnitude, which assume that spectral amplitudes increase monotonically at all periods. However, these magnitude scaling features are the natural consequence of the narrow band character of the forward rupture directivity pulse. The period of the near fault pulse is related to source parameters such as the rise time (duration of slip at a point on the fault) and the fault dimensions, which generally increase with magnitude.

Preliminary response spectral models that include the magnitude dependence of the period of the rupture directivity pulse are shown in Figure 6. These models are derived from empirical relations between pulse period and magnitude [7]. Figure 6 compares the response spectra for rock and soil predicted by this model with the standard model of Abrahamson and Silva [8], which does not explicitly include directivity effects, and the broadband model of Somerville et al. [3], whose directivity effects are based on the monotonic increase of ground motion amplitudes with magnitude at all response spectral periods. The narrowband model produces larger response spectra in the period range of about 0.5 to 2 seconds for earthquakes smaller than M_w 7.5, and smaller response spectra at all periods for earthquakes larger than M_w 7.5, compared with the broadband model.

TIME DOMAIN MODELS OF NEAR FAULT GROUND MOTIONS

The response spectrum models shown in Figure 6 do not adequately represent the demand for a high rate of energy absorption presented by near-fault pulses. Near fault ground motions containing forward rupture directivity may be simple enough to be represented by simple time

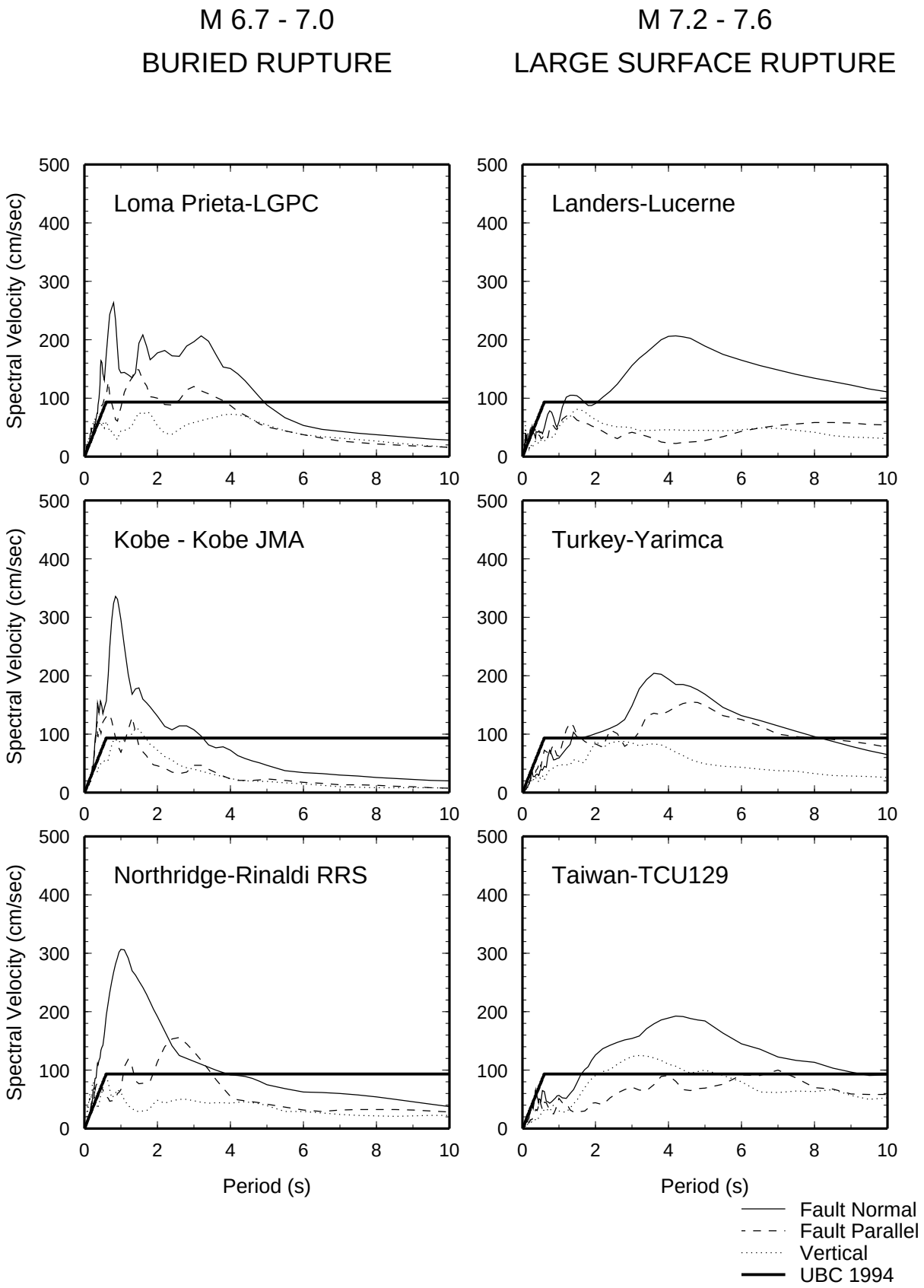

Figure 5. Spectral velocity of fault-normal pulses of moderate (left) and large (right) earthquakes.

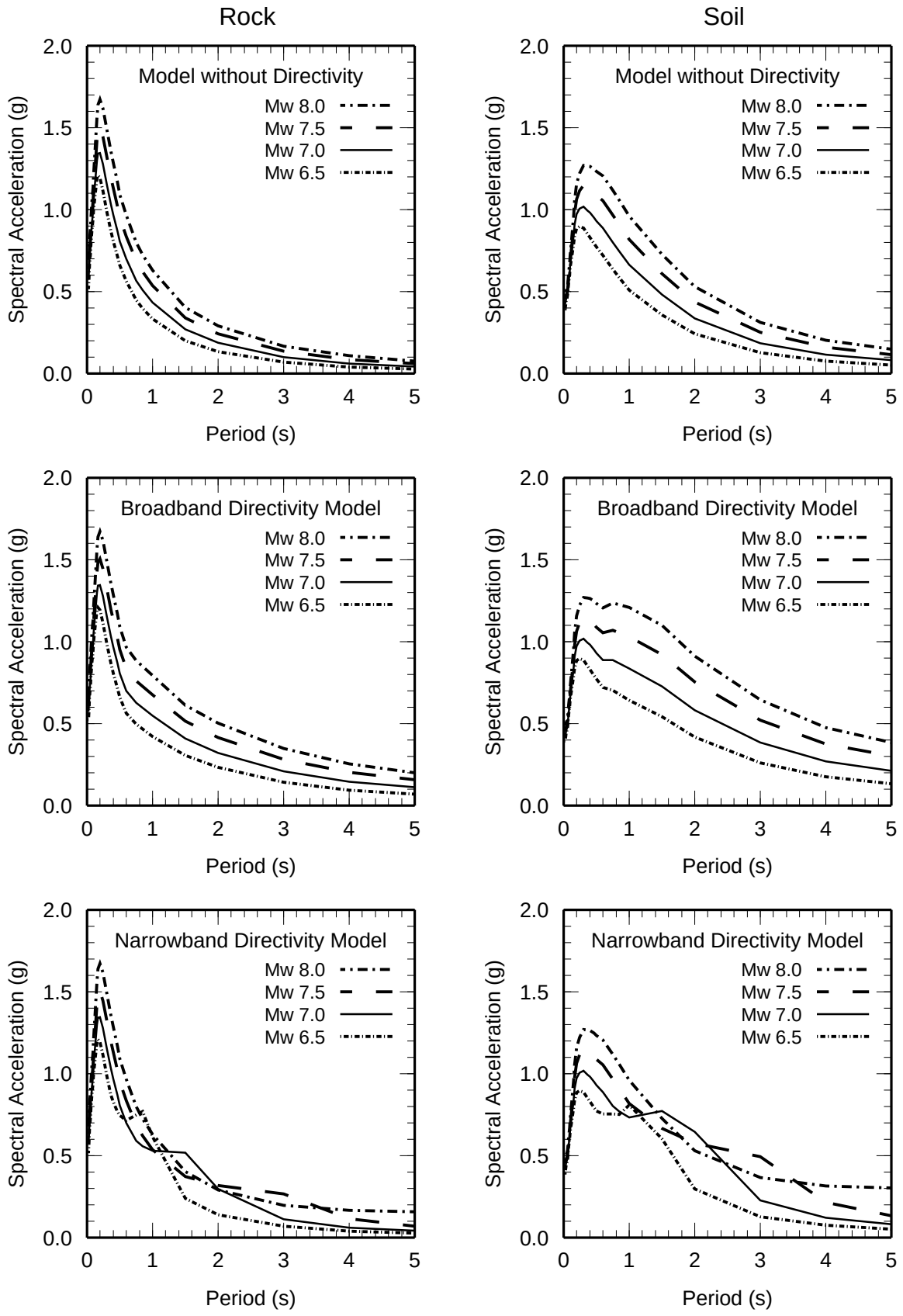

Figure 6. Near fault response spectral model, strike-slip, 5km for rock sites (left) and soil sites (right). Top: model without directivity (Abrahamson and Silva, 1997). Middle: Broadband directivity model (Somerville et al., 1997). Bottom: Narrow band directivity model (this study).

domain pulses, thus simplifying the specification of ground motion time histories for use in structural response analyses. Preliminary equations relating the period of the pulse to the earthquake magnitude, and the effective velocity of the pulse to the earthquake magnitude and distance, have been developed by Somerville [7], Somerville et al. [9], Alavi and Krawinkler [10], and Rodriguez-Marek [11]. The effect of the simultaneous dynamic and static ground motions on the response of a structure can be analyzed using time histories that include both the dynamic rupture directivity pulse and the static ground displacement.

CONCLUSIONS

Near-fault ground motions differ from ordinary ground motions in that they often contain strong coherent dynamic long period pulses and permanent ground displacements. The dynamic motions are dominated by a large long period pulse of motion that occurs on the horizontal component perpendicular to the strike of the fault, caused by rupture directivity effects. Near fault recordings from recent earthquakes indicate that this pulse is a narrow band pulse whose period increases with magnitude, as expected from theory. This magnitude dependence of the pulse period causes the response spectrum to have a peak whose period increases with magnitude, such that the near-fault ground motions from moderate magnitude earthquakes may exceed those of larger earthquakes at intermediate periods (around 1 second). The static ground displacements in near-fault ground motions, caused by the relative movement of the two sides of the fault on which the earthquake occurs, are discontinuous across a fault having surface rupture, and can subject a bridge crossing a fault to significant differential displacements. The static ground displacements occur at about the same time as the large dynamic motions, indicating that the static and dynamic displacements need to be treated as coincident loads.

REFERENCES

[1] Abrahamson, 1993. Spatial variation of multiple support inputs. *Proceedings of the first U.S. symposium on the seismic evaluation and retrofit of steel bridges*, U.C. Berkeley, October 18.

[2] Archuleta, R. J. and S. H. Hartzell, 1981. Effects of fault finiteness on near-source ground motion. *Bull. Seismol. Soc. Am*., 71: 939-957.

[3] Somerville, P.G., N.F. Smith, R.W. Graves, and N.A. Abrahamson (1997). Modification of empirical strong ground motion attenuation relations to include the amplitude and duration effects of rupture directivity, *Seismological Research Letters* 68, 199-222.

[4] Aki, K. and P.G. Richards (1980). *Quantitative Seismology: Theory and Methods*. W.H. Freeman & Co.

[5] Wells, D.L. and K.J. Coppersmith (1994). Analysis of empirical relationships among magnitude, rupture length, rupture area, and surface displacement, *Bull. Seismol. Soc. Am. 84*, 974-1002.

[6] Abrahamson, N.A., 2000. Effects of rupture directivity on probabilistic seismic hazard analysis. Proceedings of the 6th International Conference on Seismic Zonation, Palm Springs, Earthquake Engineering Research Institute.

[7] Somerville, P.G. (2001). Magnitude scaling of the near fault rupture directivity pulse. *Proceedings of the International Workshop on the Quantitative Prediction of Strong-Motion and the Physics of Earthquake Sources*, October 23-25, 2000, Tsukuba, Japan

[8] Abrahamson. N.A. and W.J. Silva, 1997. Empirical response spectral attenuation relations for shallow crustal earthquakes. *Seismological Research Letters*, 68: 94-127.

[9] Somerville, P.G., H. Krawinkler and B. Alavi, 2000. Development of improved ground motion representation and design procedures for near-fault ground motions. *Final Report to CSMIP Data Utilization Program*, Contract No. 1097-601.

[10] Alavi, B. and H. Krawinkler, 2000. Design considerations for near-fault ground motions. *Proceedings of the U.S. – Japan Workshop on the Effects of Near-Fault Earthquake Shaking*, San Francisco, March 20-21.

[11] Rodriguez-Marek, A., 2000. Near fault seismic site response. Ph.D. Thesis, Civil Engineering, University of California, Berkeley, 451 pp.